(Shizuoka, Japan). Mice were properly anesthetized during experiments.

Experimental Protocol. Six-week-old female C57BL6 mice were treated with 1 mL/kg CCl_4 dissolved in olive oil (1:1) twice a week for 4 weeks. One day (24 hours) after the eighth injection of CCl_4, 1×10^5 green fluorescent protein (GFP)-positive BMCs or sorted Liv8-positive or Liv8-negative BMCs (1×10^5 cells) or same volume of saline as a control (described also as mice treated with CCl_4 alone) were injected into the tail vein as described previously.[11,12] Mice continued to be treated with CCl_4. After 1, 2, 3, or 4 weeks, mice were then sacrificed to assess the extent of liver fibrosis. For examination of the survival rate, mice were treated with CCl_4 for 4 weeks and divided into 2 groups (15 mice each) with bone marrow transplantation or the same volume of saline injection. All mice were then treated with CCl_4 for a further 25 weeks.

BMC Preparation. For BMC isolation, GFP-transgenic mice (TgN(β-act-EGFP)Osb) (6 weeks old) were killed by cervical dislocation and the limbs removed. GFP-positive BMCs were flushed with Dulbecco's Modified Eagle medium (DMEM) culture medium with 10% fetal bovine serum (FBS) from the medullary cavities of tibias and femurs using a 25-G needle.

Production of Rat Monoclonal Antibody, Liv8. Eight-week old WKY/NCrj female rats were immunized in the hind footpads with 100 μg of E11.5 murine fetal liver lysate in complete Freund's adjuvant (0.2 mL). Anti-Liv8 antibodies were raised according to a previously described protocol.[13]

Fluorescence-Activated Cell Sorter Analysis of Fetal Liver Cells and BMCs Using Anti-Liv8 Antibody. Prepared mouse fetal liver cells (E11.5) and adult BMCs were reacted with biotin-conjugated anti-Liv8 antibody,[12] phycoerythrin-conjugated rat anti-CD45 (Becton Dickinson Bioscience, San Jose, CA), fluorescein isothiocyanate-conjugated anti–c-kit (Becton Dickinson Bioscience), phycoerythrin-conjugated anti–Thy 1 (Becton Dickinson Bioscience), and fluorescein isothiocyanate-conjugated anti-B220 antibodies (Becton Dickinson Bioscience) at the rate of 1 μg per 10^6 total cells, mixed well, and incubated in the tube for 30 to 40 minutes at 4°C. Following the incubation with the first antibody, the cells were washed twice by 0.02 mol/L phosphate-buffered saline (PBS) and centrifuged at 500*g* for 5 minutes. Labeled cells were then reacted to allophycocyanin-conjugated streptavidin (Becton Dickinson Bioscience) at the rate of 1 μg per 10^6 total cells, mixed well, and incubated in the tube for 30 to 40 minutes at 4°C. After that, these were washed out once with 0.02 mol/L PBS and centrifuged at 500*g* for 5 minutes. The labeled cells were analyzed using FACS Calibur (Becton Dickinson Bioscience).

Preparation of Liv8-positive and Liv8-negative BMCs Liv8-positive and Liv8-negative BMCs were prepared as described previously.[12] Briefly, prepared BMCs were reacted to rat anti-Liv8 immunoglobulin G (IgG) antibody at the rate of 1 μg per 10^6 total cells, mixed well, and incubated in the tube for 30 minutes at 4°C. Cells were then washed twice by 0.02 mol/L PBS and centrifuged at 500*g* for 5 minutes. Cells were labeled with rat anti-Liv8 IgG antibody by reacting with goat anti-rat IgG MicroBeads (Miltenyi Biotec GmbH, Bergisch Gladbach, Germany) at the rate of 20 μL per 10^7 total cells, mixed well, and incubated for 20 minutes at 4°C. Labeled cells were washed once by 0.02 mol/L PBS and centrifuged at 500*g* for 5 minutes. These cells were separated into Liv8-positive cells or Liv8-negative cells by the autoMACS magnetic cell sorting system (Miltenyi Biotec GmbH) for 10 minutes per tube.

Tissue Preparation and Immunohistochemistry. The liver was perfused via the heart with 4% paraformaldehyde to flush out blood cells and incubated with 4% paraformaldehyde overnight. Tissues were then soaked in 30% sucrose for 3 days. Tissues were frozen with liquid nitrogen to prepare for sectioning with a cryostat for immunohistochemistry.

Cells expressing GFP and matrix metalloproteinase (MMP)-9 (or α-smooth muscle actin) were analyzed by both fluorescent microscopy and conventional immunohistochemistry using anti-GFP, anti–MMP-9 (Santa Cruz Biotechnology, Santa Cruz, CA), and anti–α-smooth muscle actin antibodies (Sigma-Aldrich, St. Louis, MO). Tissues were soaked in 0.3% Triton X-100 with 0.05% normal goat serum (NGS) (Chemicon, Temecula, CA) or normal rabbit serum (NRS) (Chemicon) in PBS overnight. The next day, the tissues were put in 500 mL of 10% NGS or NRS in 0.3% Triton X-100 of PBS for 2 hours, then washed with 0.3% Triton X-100 with 0.05% NGS or NRS in PBS for 10 minutes. We soaked the tissues in 1.5% H_2O_2 in 50% methanol with distilled water for 2 hours. The tissues were then washed in 0.3% Triton X-100 with 0.05% NGS or NRS in PBS. Sections were incubated with anti-GFP and anti–MMP-9 (ICN Pharmaceuticals Inc., Kanagawa, Japan) antibodies. Anti–biotin-conjugated anti-goat IgG, anti-rabbit IgG, biotin-conjugated rabbit anti-goat IgG, and biotin-conjugated rabbit anti-mouse IgG were purchased from Dako Japan (Kyoto, Japan) and used as the secondary antibodies. PAP-goat (B0157), PAP-mouse (B0650), and PAP-rabbit (Z0113) polyclonal antibodies (Dako Japan) were used as third antibodies.

For fluorescent immunohistochemistry, we used Alexa Fluor R 488 and 568 donkey anti–goat- or anti–rabbit-

or anti–mouse-IgG (H + L)-conjugated antibodies (Molecular Probe Inc., Eugene, OR) as second antibodies.

For the evaluation of fibrosis, picro-sirius red staining was performed using 0.1% picro-sirius red solution as previously described.[14]

Quantitative Analysis of Liver Fibrosis. We quantified the liver fibrosis area with picro-sirius red staining using an Olympus Provis microscope equipped with a CCD camera (Tokyo, Japan), as described previously.[15] Briefly, the red area, considered the fibrotic area, was assessed by computer-assisted image analysis with MetaMorph software (Universal Imaging Corporation, Downingtown, PA) at a magnification of ×40. The mean value of 6 randomly selected areas per sample was used as the expressed percent area of fibrosis.

Microarray Analysis. Microarray analysis was performed as described previously.[16]

Briefly, total RNA of liver was isolated using the Atlas Pure Total RNA labeling system (Clontech Laboratories, Inc.) from mice 1 week after BMC transplantation (n = 3) or from mice treated with CCl_4 for 5 weeks (n = 3) according to the manufacturer's recommendations. Differential hybridization analysis was done using an Atlas Mouse complementary DNA expression array (BD Bioscience Clontech, Tokyo, Japan). Complementary DNA probe preparation and hybridization were done according to the manufacturer's recommendations. The array results were scanned with a Strom 840 PhosphoImager (Molecular Dynamics, Sunnyvale, CA) and analyzed with Atlas Image software (BD Bioscience Clontech). The results show the mean values of 3 mice in each group.

Hydroxyproline Content. Hydroxyproline content was determined by a modification of Kivirikko's method, as previously reported.[17] Briefly, liver specimens were weighed, and 20 mg of the freeze-dried sample was hydrolyzed in 6 mol/L HCl at 110°C in an autoclave at a pressure of 1.2 kg force/cm^2 for 24 hours. After centrifugation at 2,000 rpm at a temperature of 4°C for 5 minutes, 2 mL of supernatant was mixed with 50 mL of 1% phenolphthalein and 8 N KOH to obtain a total volume of 5 mL of liquid at pH of 7 to 8. Absorbance was measured at 560 nm. The hydroxyproline content of the liver was expressed as micrograms per gram of wet weight.

In Situ *Hybridization.* *In situ* hybridization was performed essentially as described previously.[18] Briefly, digoxigenin (DIG)-11-UTP–labeled single-stranded RNA probes were prepared with DIG RNA labeling mix and the corresponding T3 or T7 RNA polymerase (Boehringer Mannheim Japan, Tokyo, Japan) according to the manufacturer's instructions. The mouse MMP-9 probe was a 150–base pair fragment from the 3′ untranslated region cloned in the pBluescript (Stratagene, Tokyo, Japan) vector. *In situ* hybridization was performed on tissue sections placed on Superfrost Plus slides postfixed in 4% paraformaldehyde in PBS, rinsed in PBS containing 0.1% active diethyl pyrocarbonate, and prehybridized for 2 hours at 58°C in 50% formamide, 5 × SSC (standard saline citrate), and 40 μg of salmon-sperm DNA per milliliter. Hybridization was carried out at 58°C for 16 hours in a humid chamber with 400 ng of DIG-labeled probe per milliliter diluted in the same solution used for prehybridization. After hybridization, the sections were successively washed in 2 × SSC at room temperature for 30 minutes, 2 × SSC for 1 hour at 65°C, and 0.1 × SSC at 65°C for 1 hour. For the reaction of anti-DIG antibodies, slides were preincubated in buffer A (100 mmol/L Tris, 150 mmol/L NaCl [pH 7.5]), and then with an alkaline phosphatase-coupled anti-DIG antibody (Boehringer Mannheim Japan) diluted 1:5,000 in buffer A containing 0.5% Boehringer blocking reagent for 2 hours at room temperature. The slides were washed in buffer A and then preincubated in buffer C (100 mmol/L Tris, 50 mmol/L $MgCl_2$ [pH 9.5]). Alkaline phosphatase was then revealed as described for 16 to 24 hours at room temperature. The enzymatic reaction was stopped with Tris-ethylenediaminetetraacetic acid (EDTA) for 15 minutes. The slides were rinsed in water for several hours and then dried, cleared in xylene, and mounted directly.

In Situ *Zymography.* *In situ* zymography was performed as described.[19]

The fresh specimens of CCl_4 treated with BMC-transplanted liver tissues (1 week after BMC transplantation) were embedded without fixation in Tissue-Tek optimal cutting temperature compound (Miles, Elkhart, IN). Serial frozen sections were made using a cryostat (MicroM, Walldorf, Germany) and mounted on gelatin films that were coated with 7% gelatin solution (Fuji Photo Film, Tokyo, Japan). The films with sections were incubated for 24 hours at 37°C in a moisture chamber and stained with 1.0% amido black 10B. The gelatin in contact with the proteolytic areas of the sections was digested, and thus zones of enzymic activity were indicated by negative staining. The digested areas in the sections were compared with serial sections stained with hematoxylin-eosin. As a control, liver tissues treated with CCl_4 alone (5 weeks) were used, and the frozen sections were treated in a manner similar to that already described.

Statistical Analysis. Results are presented as the mean ± SD. Differences between groups were analyzed by 1-way ANOVA.

The survival rate was examined using the Breslow-Gehan-Wilcoxon test.

Ethical Considerations. This experiment was reviewed by the Committee of Animal Experiment Ethics at

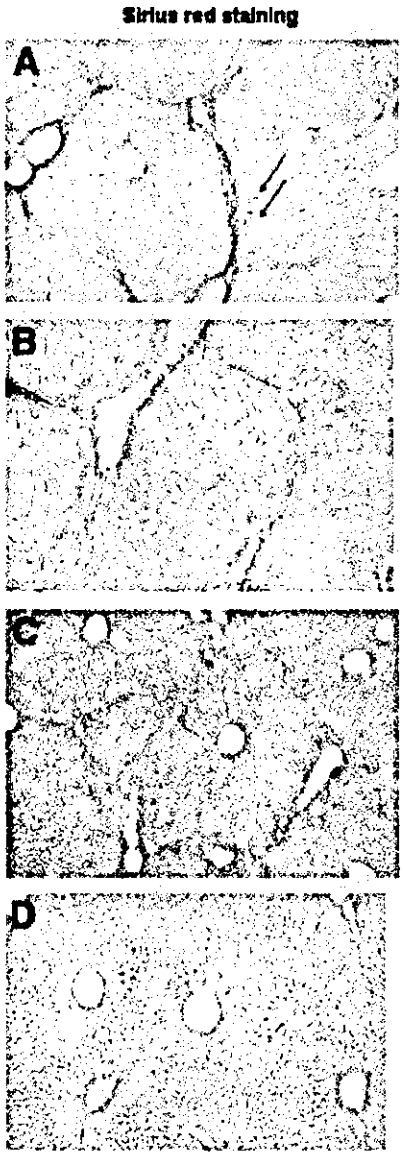

Fig. 1. Photomicrographs of liver sections stained with sirius red from mice after BMC transplantation with continuous CCl_4 treatment. Six-week-old C57BL6 mice were treated with CCl_4 twice a week for 4 weeks. Then, 1×10^5 GFP-positive BMCs were injected through the tail vein. Mice continued to be treated with CCl_4. After (A) 1, (B) 2, (C) 3, and (D) 4 weeks, mice were killed to assess the extent of liver fibrosis. (Original magnification, ×100.)

the Yamaguchi University School of Medicine and was carried out under the guidelines for animal experiments at Yamaguchi University School of Medicine (no. 105).

Results

Five weeks after CCl_4 injection, liver fibrosis was already seen (Supplementary Fig. 1A). One week after BMC transplantation (5 weeks after CCl_4 injection), BMCs were seen along with the fibers recognized by light red staining (black arrows), different from hepatocytes (Fig. 1A) with sirius red staining. More BMCs were seen after 2 weeks (Figs. 1B and 2A,C) and 3 weeks (Figs. 1C and 2B,D), and large spheroid-shaped cells (blue arrows) and small cells (green arrows) (Fig. 2B) were found in the area presumably occupied by fibers (Fig. 2D), shown by sirius red and GFP staining.

Surprisingly, 4 weeks later, the BMC-transplanted liver clearly showed reduction of liver fibrosis (Fig. 1D) compared with the liver treated with CCl_4 alone at 8 weeks (Supplementary Fig. 1D), although CCl_4 was injected throughout the experimental period. Quantitative image analysis of liver fibrosis indicated that the percent area of liver fibrosis at 1 week after BMC transplantation was 5.36% ± 0.90%, but at 4 weeks after transplantation it was significantly decreased to 4.16% ± 0.53% ($P < .001$, n = 8 each; Fig. 3).

Treatment with CCl_4 alone for 8 weeks showed an increased hydroxyproline content of 630 ± 93 μg/wet g liver (Table 1). BMC transplantation significantly reduced this to 392 ± 59 μg/wet g liver 4 weeks later ($P < .01$, n = 8 each). This hydroxyproline content was significantly reduced even compared with that of 1 week after BMC transplantation (494 ± 74 μg/wet g liver, $P < .05$).

The mouse fetal liver at E11.5 functions as a definitive hematopoietic organ, and Liv8-positive cells of the fetal liver at E11.5 include c-kit–positive immature hematopoietic cells and CD45-positive lymphoid cells. These results indicate that almost all Liv8-positive cells are of hematopoietic origin (Supplementary Fig. 2).

In addition, all c-kit–positive mouse adult BMCs belong to the Liv8-positive fraction, and Liv8-positive BMCs include almost all of the CD45- and Thy-1–positive BMCs, in addition to B220, a marker of B lymphocytes (Fig. 4).

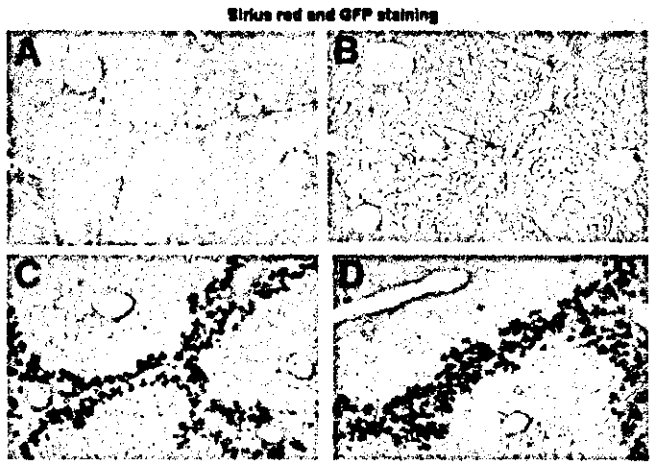

Fig. 2. Photomicrographs of liver sections stained with sirius red or sirius red and GFP from a mouse (A, C) 2 weeks and (B, D) 3 weeks after BMC transplantation. (Original magnification, [A] ×200; [B] ×200; [C] ×200; [D] ×200.)

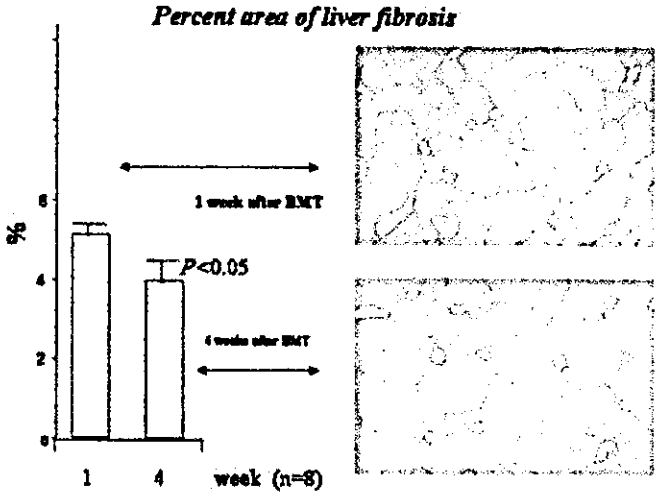

Fig. 3. Quantitatitve analysis of liver fibrosis after bone marrow cell transplantation (BMT). Percent area of liver fibrosis was calculated using sirius red staining as described in Materials and Methods. Results are expressed as mean ± SD of 8 samples. (Original magnification, ×40.)

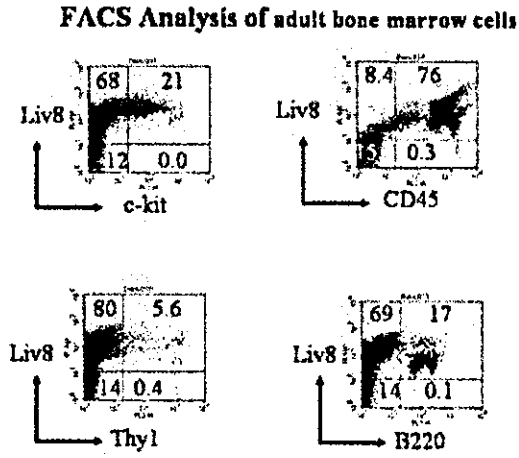

Fig. 4. Expression of Liv8, c-kit, CD45, Thy 1, and B220 in adult BMCs.

These results strongly suggest that Liv8-positive cells include both immature and mature hematopoietic cells.

Liv8-negative BMCs significantly reduced liver fibrosis compared with that of the liver treated with CCl4 alone for 8 weeks, although Liv8-positive BMCs had no effect on liver fibrosis (Table 2).

Microarray analysis of the liver 1 week after BMC transplantation indicated increased expression of MMP-2, MMP-9 and MMP-14 with decreased expression of tissue inhibitor of metalloproteinase-3 (TIMP-3) compared with that of the liver treated with CCl_4 alone for 5 weeks (Table 3). Because the expression of MMP-9 was marked, we investigated it in this model.

Immunohistochemistry of MMP-9 showed localization of these cells similar to that of transplanted BMCs (Fig. 5A). However, the liver treated with CCl_4 alone showed only a few MMP-9–positive nonparenchymal cells (black arrows, Fig. 5B).

The expression of MMP-9 with *in situ* hybridization coincided with the immunohistochemical staining of MMP-9 (Fig. 5C).

Table 1. Hydroxyproline Content

Treatment (No. of Mice)	Hydroxyproline (μg/g Liver)
CCl_4, 5 wk (8)	464 ± 93
CCl_4, 8 wk (8)	630 ± 93
CCl_4/BMT, 5 wk (8)	494 ± 74
CCl_4/BMT, 8 wk (8)	392 ± 59*†

NOTE. Mice were treated with CCl_4 for 4 weeks; then, 1 week or 4 weeks after bone marrow cell transplantation (BMT) or saline injection with CCl_4 treatment, they were killed to measure liver hydroxyproline content. Results are typical of 1 of 3 independent experiments.

*$P < .01$ vs. CCl_4 (8 weeks).

†$P < .05$ vs. CCl_4/BMT (5 weeks).

Although double fluorescent-positive cells were not seen in the liver treated with CCl_4 alone (Fig. 6A), double-positive yellow-colored cells (black arrows) were seen in the BMC-transplanted liver (Fig. 6B). With high magnification, double fluorescent immunohistochemistry showed the expression of MMP-9 (red) on the GFP-positive (green) cell surface (Fig. 6C).

A double fluorescent (anti-GFP with green color and anti–α-smooth muscle actin with red color) study indicated that a fine network pattern of stellate cells (red) existed in the liver treated with CCl_4 alone for 5 weeks (Fig. 7A). Conversely, GFP-positive green-colored cells (green arrow) were seen with a reduced fine network pattern (red arrow) in the liver 1 week after BMC transplantation (Fig. 7B). Double fluorescent-positive yellow-colored cells (yellow arrow), presumably stellate cells, were then seen without the fine network pattern (red arrow) in the liver 2 weeks after BMC transplantation (Fig. 7C). The shape of these cells was different from other GFP-positive cells, and the number of the double-positive cells was very small.

Next, we examined the direct activity of MMP-9 using *in situ* zymography. Film *in situ* zymographic analysis revealed strong gelatinolytic activity in the periportal area

Table 2. Hydroxyproline Content

Treatment (No. of mice)	Hydroxyproline (μg/g Liver)
CCl_4 (8)	687 ± 102
CCl_4/Liv8-positive (8)	638 ± 94
CCl_4/Liv8-negative (8)	415 ± 77*

NOTE. Mice were treated with CCl_4 for 4 weeks followed by transplantation with Liv8-positive or Liv8-negative BMCs or saline. After 4 weeks of CCl_4 treatment (total 8 weeks), mice were killed to measure liver hydroxyproline content. Results are typical of 1 of 3 independent experiments.

*$P < .01$ vs. CCl_4.

Table 3. Microarray Analysis

	CCl_4 + BMC vs. CCl_4 Alone	
	Increased	Decreased
MMP-2	1.7	
MMP-9	3.9	
MMP-14	2.1	
TIMP-3		0.67

NOTE. Mice were treated with CCl_4 for 4 weeks and were killed 1 week after BMC transplantation. Microarray analysis was performed using 3 livers from each group. The expression ratios (CCl_4 + BMC vs. CCl_4 alone) larger than 1.5 are shown. Values indicated are the difference between the mean values of 3 mice. Results are typical of 1 of 2 independent experiments.

coinciding with the location of MMP-9–positive BMCs compared with the liver treated with CCl_4 alone (Fig. 8).

This gelatinolytic activity was completely blocked by the addition of 1,10-phenanthroline, an MMP inhibitor (data not shown).

Finally, the mice that underwent BMC transplantation with continuous CCl_4 injection showed a gradually increased serum albumin level (Supplementary Fig. 3) resulting in a significantly improved survival rate after BMC transplantation compared with mice treated with CCl_4 alone (Supplementary Fig. 4).

Discussion

In this report, transplanted BMCs can degrade collagen fibers and clearly reduce liver fibrosis with strong expression of MMPs, especially MMP-9, as indicated by both *in situ* zymography and the double staining of GFP and MMP-9 using fluorescent microscopy. The reason for the strong expression of MMP-9 is still unknown.

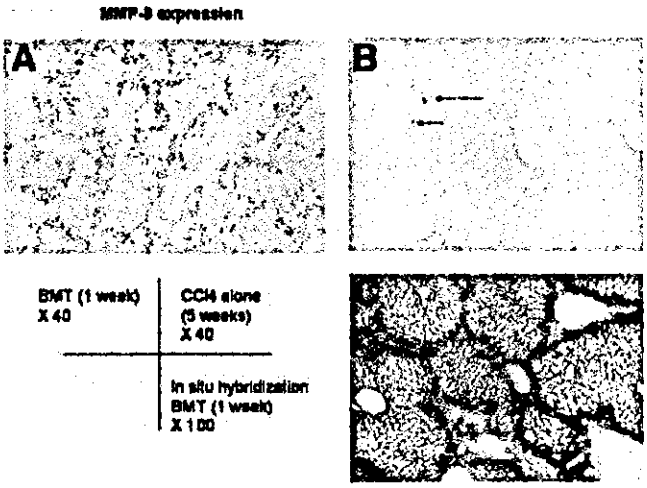

Fig. 5. Photomicrograph of a liver section stained with anti-MMP-9 antibody (A) from a mouse 1 week after BMC transplantation (BMT) and (B) from a mouse treated with CCl_4 alone for 5 weeks. (Original magnification, ×40.) (C) *In situ* hybridization of a liver section from a mouse 1 week after BMC transplantation. (Original magnification, ×100.)

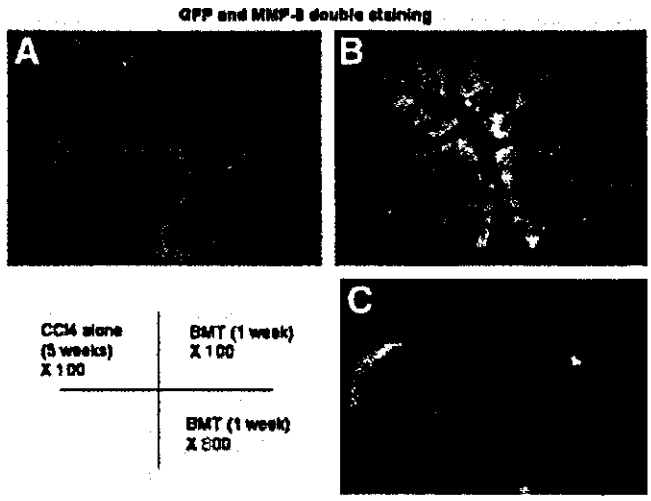

Fig. 6. Double fluorescent immunohistochemistry of a mouse liver after (A) 5-week treatment with CCl_4 alone and (B, C) 1 week after BMC transplantation (BMT) with CCl_4 treatment for 5 weeks. (Original magnification, [A and B] ×100; [C] ×800.)

However, Heissing et al.[20,21] recently reported that MMP-9 induced in BMCs released soluble Kit-ligand, which might be related to the transfer of stem cells in BMCs to the proliferative niche. Therefore, MMP-9 in our model could play an important role in the degradation of extracellular matrix and also by releasing some factors, *e.g.*, soluble Kit-ligand, related to the differentiation and proliferation of transplanted BMCs in liver inflammation induced by continuous injection of CCl_4. It has also been shown that MMP-9 plays an important role in the migration of mast progenitor cells to inflammatory

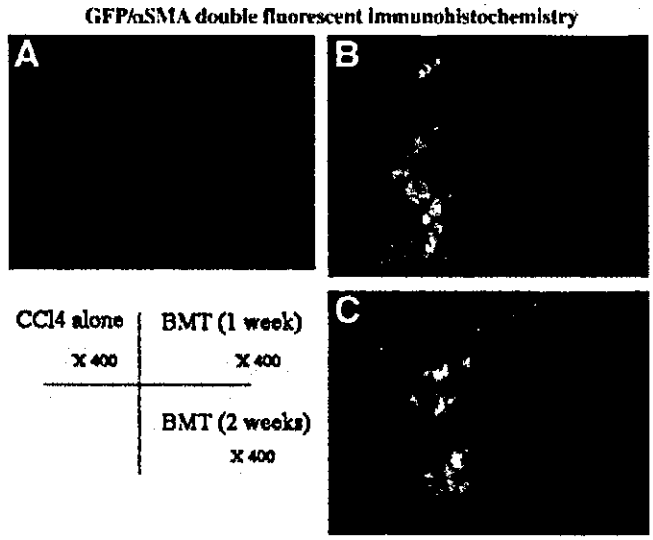

Fig. 7. Double fluorescent immunohistochemistry for α-smooth muscle actin (αSMA) and GFP of a mouse liver (A) treated with CCl_4 alone for 5 weeks and (B) 1 week, or (C) 2 weeks after BMC transplantation (BMT) with CCl_4 treatment. (Original magnification, ×400.)

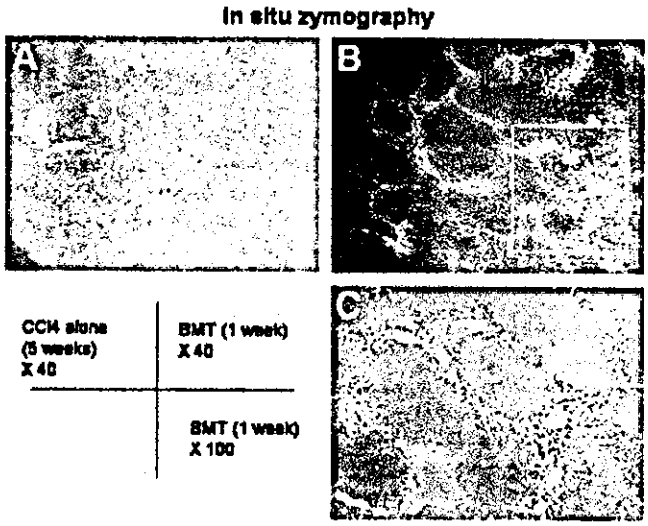

Fig. 8. *In situ* zymography of a mouse liver after (A) 5-week treatment with CCl_4 alone and (B, C) 1 week after BMC transplantation (BMT) with CCl_4 treatment for 5 weeks. (Original magnification, [A] ×40; [B] ×40, [C] ×100.)

tissue.[22,23] Therefore, the increased expression of MMP-9 in this study was somehow related to the migration of BMCs to the inflammatory liver.

Film *in situ* zymography clearly showed that these MMP-9–positive cells possessed high gelatinolytic activity compared with the liver treated with CCl_4 alone. Thus, the BMCs that migrated acted in the degradation of liver fibrosis (fibrolysis).

According to our present data, increased expression of MMP-14 (MT1-MMP [membrane-type 1 matrix metalloproteinase]) will contribute to degrading interstitial collagens[24] to gelatin that MMP-9 can degrade, resulting in the regression of fibrosis (fibrolysis).

Recently, Kollet et al.[25] reported that the expression of MMP-9 was increased with the migration of human $CD34^+$ progenitor cells in CCl_4-treated NOD/SCID mice and that an inhibitor of MMP-9 reduced this migration. Thus, proteolytic activity seems to be necessary for the cell migration in addition to matrix degradation activity.

It seems to be very important how many cells can migrate into the damaged liver to degrade fibers, but a recent paper[26] reported little evidence of bone marrow-derived hepatocytes in the CCl_4-treated liver. However, the dose of CCl_4 was only 4% (0.08 mL/kg) of our dose (0.5 mL/kg), and the number of mice used was too small (1 or 2). The reason they did not see the BMCs that migrated is most likely due to the cessation of CCl_4 injection after BMC transplantation. Even in our experimental model,[11] the cessation of CCl_4 after BMC transplantation dramatically reduced the number of BMCs migrating into the damaged liver (I.S., unpublished data, 2003). Thus, the extent of continuing liver damage may limit BMC migration to the liver with matrix degradation activity.

Transplanted BMCs differentiated into albumin-producing hepatocytes with an increased serum albumin level, and the degradation of the extracellular matrix may presumably lead to improved liver function resulting in better survival of mice with BMCtransplantation compared to that of treated with CCl_4 alone, although only 1 transplantation of BMCs was performed.

As shown by double fluorescence, our data may also indicate that transplanted BMCs seem to become stellate cells, in agreement with a recent report,[27] although the number was very small in our experimental model. This result seems to be contradictory to our result of resolution of liver fibrosis by BMC transplantation because transdifferentiated stellate cells may produce collagens. Our preliminary results indicated reduced messenger RNA expression of type I procollagen, transforming growth factor-β1 (TGF-β1) and no change of hepatocyte growth factor messenger RNA expression in the liver 1 week after BMC transplantation compared with the liver treated with CCl_4 alone (I. Sakaida, unpublished data, 2003). As shown in Fig. 7, migrated BMCs seemed to reduce the fine network pattern of activated stellate cells. Thus, transplanted BMCs may affect activated stellate cells by reducing their number—*e.g.*, by leading them to apoptosis. However, further examinations are necessary to determine the exact relationship between BMCs and resident stellate cells.

Our recent data[12] indicated that the subpopulation of BMCs, nonhematopoietic cells in bone marrow, separated using an anti-Liv8 antibody, will transdifferentiate into hepatocytes in the liver damaged by CCl_4 induction. The present study clearly indicates that this subpopulation of BMCs is also responsible for the resolution of liver fibrosis (fibrolysis) induced by CCl_4 treatment.

In conclusion, the present study introduces a new concept for the treatment of liver fibrosis.

References

1. Petersen BE, Bowen WC, Patrene KD, Mars WM, Sullivan AK, Murase N, et al. Bone marrow as a potential source of hepatic oval cells. Science 1999;284:1168–1170.
2. Theise ND, Nimmakayalu M, Gardner R, Illei PB, Morgan G, Teperman L, et al. Liver from bone marrow in humans. HEPATOLOGY 2000;32:11–16.
3. Alison MR, Poulsom R, Jeffery R, Dhillon AP, Quaglia A, Jacob J, et al. Hepatocytes from nonhepatic adult stem cells. Nature 2000;406:257.
4. Krause DS, Theise ND, Collector MI, Henegariu O, Hwang S, Gardner R, et al. Multi-organ, multi-lineage engraftment by a single bone marrow-derived stem cell. Cell 2001;105:369–377.
5. Lagasse E, Connors H, Al-Dhalimy M, Reitsma M, Dohse M, Osborne L, et al. Purified hematopoietic stem cells can differentiate into hepatocytes in vivo. Nat Med 2000;6:1229–1234.

6. Orlic D, Kajstura J, Chimenti S, Jakoniuk I, Anderson SM, Li B, et al. Bone marrow cells regenerate infarcted myocardium. Nature 2001;410: 701–705.
7. Korbling M, Katz RL, Khanna A, Ruifrok AC, Rondon G, Albitar M, et al. Hepatocytes and epithelial cells of donor origin in recipients of peripheral-blood stem cells. N Engl J Med 2002;346:738–746.
8. Okamoto R, Yajima T, Yamazaki M, Kanai T, Mukai M, Okamoto S, et al. Damaged epithelia regenerated by bone marrow-derived cells in the human gastrointestinal tract. Nat Med 2002;8:1011–1017.
9. Wagers AJ, Sherwood RI, Christensen JL, Weissman IL. Little evidence for developmental plasticity of adult hematopoietic stem cells. Science 2002; 297:2256–2259.
10. Okabe M, Ikawa M, Kominami K, Nakanishi T, Nishimune Y. "Green mice" as a source of ubiquitous green cells. FEBS Lett 1997;407:313–319.
11. Terai S, Sakaida I, Yamamoto N, Omori K, Watanabe T, Ohata S, et al. An in vivo model for monitoring trans-differentiation of bone marrow cells into functional hepatocytes. J Biochem (Tokyo). 2003;134:551–558.
12. Yamamoto N, Terai S, Ohata S, Watanabe T, Omori K, Shinoda K, et al. A subpopulation of bone marrow cells depleted by a novel antibody, anti-Liv8, is useful for cell therapy to repair damaged liver. Biochem Biophys Res Commun 2004;313:1110–1118.
13. Watanabe T, Nakagawa K, Ohata S, Kitagawa D, Nishitai G, Seo J, et al. SEK1/MKK4-mediated SAPK/JNK signaling participates in embryonic hepatoblast proliferation via a pathway different from NF-kappaB-induced anti-apoptosis. Dev Biol 2002;250:332–347.
14. Sakaida I, Uchida K, Matsumura Y, Okita K. Interferon gamma treatment prevents procollagen gene expression without affecting transforming growth factor-beta1 expression in pig serum-induced rat liver fibrosis in vivo. J Hepatol 1998;28:471–479.
15. Sakaida I, Nagatomi A, Hironaka K, Uchida K, Okita K. Quantitative analysis of liver fibrosis and stellate cell changes in patients with chronic hepatitis C after interferon therapy. Am J Gastroenterol 1999;94:489–496.
16. Sakaida I, Tsuchiya M, Kawaguchi K, Kimura T, Terai S, Okita K. Herbal medicine Inchin-ko-to (TJ-135) prevents liver fibrosis and enzyme-altered lesions in rat liver cirrhosis induced by a choline-deficient L-amino acid-defined diet. J Hepatol 2003;38:762–769.
17. Sakaida I, Hironaka K, Uchida K, Suzuki C, Kayano K, Okita K. Fibrosis accelerates the development of enzyme-altered lesions in the rat liver. HEPATOLOGY 1998;28:1247–1252.
18. Jimenez MJ, Balbin M, Lopez JM, Alvarez J, Komori T, Lopez-Otin C. Collagenase 3 is a target of Cbfa1, a transcription factor of the runt gene family involved in bone formation. Mol Cell Biol 1999;19:4431–4442.
19. Nakada M, Nakamura H, Ikeda E, Fujimoto N, Yamashita J, Sato H, et al. Expression and tissue localization of membrane-type 1, 2, and 3 matrix metalloproteinases in human astrocytic tumors. Am J Pathol 1999;154: 417–428.
20. Heissig B, Hattori K, Dias S, Friedrich M, Ferris B, Hackett NR, et al. Recruitment of stem and progenitor cells from the bone marrow niche requires MMP-9 mediated release of kit-ligand. Cell 2002;109:625–637.
21. Hattori K, Heissig B, Wu Y, Dias S, Tejada R, Ferris B, et al. Placental growth factor reconstitutes hematopoiesis by recruiting VEGFR1(+) stem cells from bone-marrow microenvironment. Nat Med 2003;8:841–849.
22. Tanaka A, Arai K, Kitamura Y, Matsuda H. Matrix metalloproteinase-9 production, a newly identified function of mast cell progenitors, is down-regulated by c-kit receptor activation. Blood 1999;94:2390–2395.
23. Baram D, Vaday GG, Salamon P, Drucker I, Hershkoviz R, Mekori YA. Human mast cells release metalloproteinase-9 on contact with activated T cells: juxtacrine regulation by TNF-alpha. J Immunol 2001;167:4008–4016.
24. Ohuchi E, Imai K, Fujii Y, Sato H, Seiki M, Okada Y. Membrane type 1 matrix metalloproteinase digests interstitial collagens and other extracellular matrix macromolecules. J Biol Chem 1997;272:2446–2451.
25. Kollet O, Shivtiel S, Chen YQ, Suriawinta J, Thung SN, Dabeva MD, et al. HGF, SDF-1, and MMP-9 are involved in stress-induced human CD34+ stem cell recruitment to the liver. J Clin Invest 2003;112:160–169.
26. Kanazawa Y, Verma IM. Little evidence of bone marrow-derived hepatocytes in the replacement of injured liver. Proc Natl Acad Sci U S A 2003; 100(Suppl);11850–11853.
27. Forbes SJ, Russo FP, Rey V, Burra P, Rugge M, Wright NA, et al. A significant proportion of myofibroblasts are of bone marrow origin in human liver fibrosis. Gastroenterology 2004;126:955–963.

Available online at www.sciencedirect.com
SCIENCE DIRECT
Toxicology Letters 152 (2004) 175–181
Toxicology Letters
www.elsevier.com/locate/toxlet

Requirement of MKK4 and MKK7 for $CdCl_2$- or $HgCl_2$-induced activation of c-Jun NH_2-terminal kinase in mouse embryonic stem cells

Masato Matsuoka [a,b,*], Hideki Igisu [b], Kentaro Nakagawa [c], Toshiaki Katada [c], Hiroshi Nishina [c]

[a] *Department of Hygiene and Public Health (1), School of Medicine, Tokyo Women's Medical University, 8-1 Kawada-cho, Shinjuku-ku, Tokyo 162-8666, Japan*
[b] *Department of Environmental Toxicology, Institute of Industrial Ecological Sciences, University of Occupational and Environmental Health, 1-1 Iseigaoka, Yahatanishi-ku, Kitakyushu 807-8555, Japan*
[c] *Department of Physiological Chemistry, Graduate School of Pharmaceutical Sciences, University of Tokyo, 7-3-1 Hongo, Bunkyo-ku, Tokyo 113-0033, Japan*

Received 10 March 2004; received in revised form 27 April 2004; accepted 28 April 2004

Available online 15 June 2004

Abstract

c-Jun NH_2-terminal kinase (JNK), also known as stress-activated protein kinase (SAPK), is activated primarily by inflammatory cytokines and environmental stresses including toxic metal exposure. To reveal the upstream kinase responsible for JNK activation by toxic metals, the phosphorylation status and the activity of JNK were examined in mouse embryonic stem (ES) cells lacking MKK4 or MKK7 following exposure to $CdCl_2$ or $HgCl_2$. Treatment with $CdCl_2$ or $HgCl_2$ induced the phosphorylation of JNK in a dose- and time-dependent manner in wild-type ES cells. In both *mkk4*$^{-/-}$ and *mkk7*$^{-/-}$ ES cells, $CdCl_2$- or $HgCl_2$-induced phosphorylation and activation of JNK were suppressed significantly. However, in *mkk7*$^{-/-}$ ES cells treated with $CdCl_2$ and $HgCl_2$, JNK activation was not abolished (suppressed by 56% and 78%, respectively). These findings suggest that the full activation of JNK by toxic metal exposure requires both MKK4 and MKK7, and these upstream kinases might contribute differentially in JNK activation between mouse ES cells exposed to $CdCl_2$ and $HgCl_2$.

Keywords: c-Jun NH_2-terminal kinase; MKK4; MKK7; $CdCl_2$; $HgCl_2$; ES cells

1. Introduction

Mitogen-activated protein kinases (MAPKs) are a family of Ser/Thr protein kinases that transmit signals into the nucleus, and have been shown to participate in a diverse array of cellular functions such as the control of gene expression, cell proliferation, differentiation, development, inflammatory response, and

Abbreviations: JNK, c-Jun NH_2-terminal kinase; SAPK, stress-activated protein kinase; ES, embryonic stem; MAPK, mitogen-activated protein kinase; ERK, extracellular signal-regulated protein kinase

* Corresponding author. Tel.: +81-3-3353-8111; fax: +81-3-5269-7419.
E-mail address: matsuoka@research.twmu.ac.jp (M. Matsuoka).

0378-4274/$ – see front matter © 2004 Elsevier Ireland Ltd. All rights reserved.
doi:10.1016/j.toxlet.2004.04.033

apoptosis in mammalian systems (Chang and Karin, 2001; Weston and Davis, 2002). c-Jun NH_2-terminal kinase (JNK), also known as stress-activated protein kinase (SAPK), represents one subgroup of MAPKs that is activated primarily by inflammatory cytokines and environmental stresses such as ultraviolet radiation, ionizing radiation, heat shock, osmotic shock, protein synthesis inhibitor, and chemical mutagens (Kyriakis and Avruch, 1996; Robinson and Cobb, 1997). In addition, we have found that environmentally contaminating toxic metals such as cadmium (Matsuoka and Igisu, 1998), inorganic mercury (Matsuoka et al., 2000), and tributyltin (Yu et al., 2000) activate JNK pathway. However, functions and molecular mechanisms of toxic metal-induced JNK activation have not yet been known.

For the activation, JNK requires the dual phosphorylation of Thr and Tyr residues located in a Thr-Pro-Tyr motif between kinase subdomains VII and VIII (Cobb and Goldsmith, 1995). This phosphorylation is catalyzed by the dual specific kinases MKK4 (also known as SEK1 or MEK4) and MKK7 (SEK2), while MKK4 has a preference for the Tyr residue and MKK7 for the Thr residue (Weston and Davis, 2002). In vitro, JNK is activated synergistically by these two upstream kinases (Lawler et al., 1998). With respect to cadmium, it has been reported that JNK activation was suppressed partially by expression of dominant negative mutant of MKK7, but not that of MKK4 in human non-small-cell lung carcinoma cells (Chuang and Yang, 2001; Chuang et al., 2000) and rat mesangial cells (Ding and Templeton, 2000). These findings suggest that cadmium might activate JNK through MKK7, but not MKK4 in vivo. On the other hand, the activation of JNK by ultraviolet, heat shock, sorbitol-induced osmolarity change, or the protein synthesis inhibitor anisomycin was markedly attenuated in mouse embryonic stem (ES) cells targeting either the *mkk4* or the *mkk7* gene (Kishimoto et al., 2003), indicating that both MKK4 and MKK7 are required for the activation of JNK by these stimuli in mouse ES cells. To clarify whether signaling pathway leading to JNK activation by toxic metals is distinct from the case of other cellular stresses, the phosphorylation status and the activity of JNK were examined in $mkk4^{-/-}$ and $mkk7^{-/-}$ ES cells following exposure to $CdCl_2$ or $HgCl_2$. The application of these ES cells lacking either MKK4 or MKK7 would be more beneficial than other cells expressed with dominant negative form of them.

2. Materials and methods

2.1. Cell culture and treatments

The murine ES cell line E14K (wild-type), $mkk4^{-/-}$ mutant cell line made by the *mkk4* gene targeting (Nishina et al., 1997), and $mkk7^{-/-}$ mutant cell line made by the *mkk7* gene targeting (Kishimoto et al., 2003) were maintained in Dulbecco's modified Eagle's medium supplemented with 15% fetal calf serum (GIBCO, Invitrogen Corp., Carlsband, CA, USA) and leukemia inhibitory factor as described previously (Kishimoto et al., 2003). Wild-type, $mkk4^{-/-}$ and $mkk7^{-/-}$ ES cells (passage number 10–15) were plated at 5×10^5 cells per well (for Western immunoblotting) or 1.6×10^6 cells per well (for JNK activity assay) in six-well culture plates coated with 1% gelatin, and cultured for overnight. Then, medium was changed to serum-free medium containing $CdCl_2$ (Sigma Chemical Co., St. Louis, MO, USA) or $HgCl_2$ (Nacalai Tesque, Osaka, Japan). Untreated control cells were incubated with serum-free medium, and were treated identically to cells incubated with $CdCl_2$ or $HgCl_2$. Initially, dose (1 μM, 5 μM, 10 μM, 20 μM, or 40 μM) and time (5 min, 15 min, 30 min, 45 min, or 60 min) of $CdCl_2$ or $HgCl_2$ exposure for the sufficient induction of JNK phosphorylation were determined in wild-type ES cells. Based on these experiments, each ES cell line was incubated with 20 μM of $CdCl_2$ or $HgCl_2$ for 1 h. All experiments were repeated three (for Western immunoblotting) or four times (for JNK activity assay). Data were all obtained from two independently derived ES cell clones with comparable results.

2.2. Western immunoblotting

After the incubation with $CdCl_2$ or $HgCl_2$, ES cells were washed with phosphate-buffered saline, and lysed with sodium dodecyl sulfate (SDS)-polyacrylamide gel Laemmli sample buffer. Cell lysates were collected, sonicated, and boiled for 5 min. Twenty micrograms of protein was subjected to SDS-polyacrylamide gel electrophoresis on a 10%

polyacrylamide gel and transferred to a nitrocellulose membrane (Hybond-ECL, Amersham Pharmacia Biotech, Buckinghamshire, England). The membrane was blocked with 5% non-fat milk or bovine serum albumin in Tris-buffered saline containing 0.1% Tween 20 for 1 h at room temperature. The membrane was incubated overnight at 4 °C with the primary antibody diluted 1:1000. The antibodies used were phospho-SAPK/JNK (Thr^{183}/Tyr^{185}) antibody, phosphorylation state-independent SAPK/JNK antibody, phospho-p38 MAPK (Thr^{180}/Tyr^{182}) antibody, phosphorylation state-independent p38 MAPK antibody, phospho-p44/42 MAPK (Thr^{202}/Tyr^{204}) antibody, phosphorylation state-independent p44/42 MAPK antibody, phospho-specific c-Jun (Ser^{63}) antibody (Cell Signaling Technology, Inc., Beverly, MA, USA), anti-ACTIVE JNK antibody (Promega Corporation, Madison, IL, USA), MEK-4 (C-20) antibody (Santa Cruz Biotechnology Inc., Santa Cruz, CA, USA), and rat monoclonal antibody against MKK7 (KN-004) prepared by Kishimoto et al. (2003). Protein was detected with a Phototope-HRP Western blot detection kit (Cell Signaling Technology). For the detection of MKK7 protein, a SuperSignal West Femto Maximum Sensitivity Substrate (Pierce Chemical Co., Rockford, IL, USA) was used. After the immunodetection, some blots were incubated with a Restore Western Blot Stripping Buffer (Pierce) for 30 min at room temperature, and reprobed with each phosphorylation state-independent MAPK antibody. The bands on the developed films were quantified with NIH Image Version 1.63.

2.3. JNK activity assay

The in vitro activity of JNK was measured using a SAPK/JNK assay kit (Cell Signaling Technology) according to the instruction from the manufacturer. Briefly, cell lysates were incubated with GST-c-Jun (1–89) fusion protein overnight, and the precipitated JNK was subjected to in vitro kinase assay using GST-c-Jun (1–89) as substrate. Phosphorylation of GST-c-Jun on Ser^{63} was analyzed with immunoblotting using phospho-c-Jun antibody. The bands on the developed films were quantified with NIH Image Version 1.63.

2.4. Statistical analysis

Results were expressed as mean ± S.D. The statistical significance was determined by one-way analysis of variance followed by the Dunnett multiple comparison test. $P < 0.05$ was considered as statistically significant.

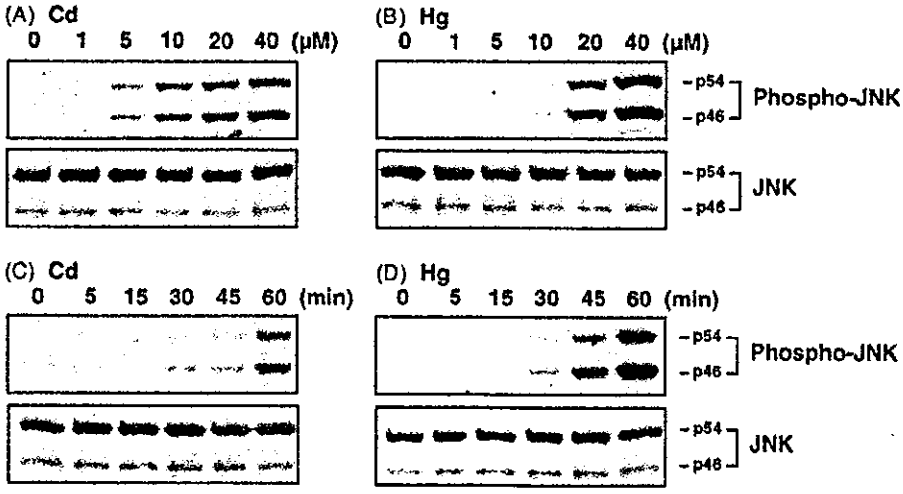

Fig. 1. Dose effects (A, B) and time course (C, D) of $CdCl_2$- or $HgCl_2$-induced accumulation of phosphorylated JNK in wild-type ES cells. Wild-type ES cells were incubated with 0 μM, 1 μM, 5 μM, 10 μM, 20 μM, or 40 μM $CdCl_2$ (A) or $HgCl_2$ (B) for 1 h. In the time course study, cells were incubated with 20 μM $CdCl_2$ (C) or $HgCl_2$ (D) for 5–60 min. The untreated control is 0 min. Cell lysates were subjected to immunoblotting using anti-phospho-JNK and anti-JNK antibodies. Results shown are representative of three independent experiments.

3. Results

3.1. $CdCl_2$- or $HgCl_2$-induced accumulation of phosphorylated JNK in wild-type ES cells

When wild-type ES cells were incubated with 5 μM of $CdCl_2$ or 20 μM of $HgCl_2$ for 1 h, phosphorylation of JNK (p46 and p54) was found, and the levels of phosphorylated form of JNK increased in a concentration-dependent manner (Fig. 1A and B). In contrast, the levels of total (phosphorylation state-independent) JNK were not changed by incubation with any concentration of $CdCl_2$ or $HgCl_2$. In the time course study, the levels of phosphorylated JNK increased after 30 min or 45 min in response to 20 μM $CdCl_2$ or $HgCl_2$ exposure, whereas total JNK levels were not changed (Fig. 1C and D). Thereafter, ES cells were exposed to $CdCl_2$ or $HgCl_2$ for 1 h at a concentration of 20 μM.

3.2. Suppression of $CdCl_2$- or $HgCl_2$-induced JNK activation in $mkk4^{-/-}$ and $mkk7^{-/-}$ ES cells

As shown in Fig. 2, MKK4 and MKK7 proteins were not detected in $mkk4^{-/-}$ and $mkk7^{-/-}$ ES cells, respectively. Neither MKK4 expression in wild-type and $mkk7^{-/-}$ ES cells nor MKK7 expression in wild-type and $mkk4^{-/-}$ ES cells was affected by the treatment with $CdCl_2$ or $HgCl_2$. In $mkk4^{-/-}$ ES cells, $CdCl_2$- or $HgCl_2$-induced phosphorylation of JNK was abolished almost completely without changing JNK levels (Fig. 3A, lanes 5 and 6). While toxic

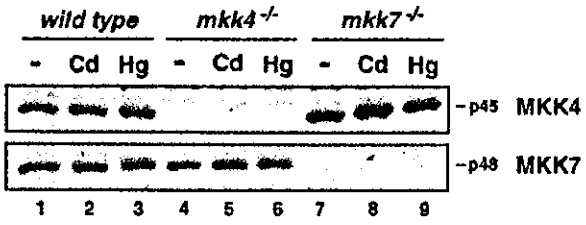

Fig. 2. Effects of $CdCl_2$ or $HgCl_2$ treatment on the levels of MKK4 and MKK7 in wild-type, $mkk4^{-/-}$ and $mkk7^{-/-}$ ES cells. Wild-type, $mkk4^{-/-}$ and $mkk7^{-/-}$ ES cells were incubated with serum-free medium (lanes 1, 4, and 7), 20 μM $CdCl_2$ (lanes 2, 5, and 8) or 20 μM $HgCl_2$ (lanes 3, 6, and 9) for 1 h, and cell lysates were subjected to immunoblotting using anti-MKK4 and anti-MKK7 antibodies. Results shown are representative immunoblot of three independent experiments.

metal-induced JNK phosphorylation in $mkk7^{-/-}$ ES cells was also reduced significantly, JNK phosphorylation in $mkk7^{-/-}$ ES cells treated with $CdCl_2$ and $HgCl_2$ was 55% and 33% of that in wild-type ES cells treated, respectively (Fig. 3A, lanes 8 and 9). These findings were reproducible with two different anti-phospho-JNK antibodies used in the present study. In contrast to JNK, substantial phosphorylation of other members of MAPK family, p38 and extracellular signal-regulated protein kinase (ERK2/p42 and ERK1/p44), were observed in both, $mkk4^{-/-}$ and $mkk7^{-/-}$ ES cells treated with $CdCl_2$ or $HgCl_2$ (Fig. 3B and C, lanes 5, 6, 8 and 9).

The in vitro activity of JNK assayed using GST-c-Jun as substrate was also examined. Treatment with $CdCl_2$ or $HgCl_2$ induced the marked elevation of JNK activity in wild-type ES cells (Fig. 4, lanes 2 and 3). Consistent with the reduction of phosphorylated JNK levels (Fig. 3A), $CdCl_2$- or $HgCl_2$-induced JNK activation was suppressed in both $mkk4^{-/-}$ and $mkk7^{-/-}$ ES cells. JNK activity in $mkk4^{-/-}$ ES cells treated with $CdCl_2$ and $HgCl_2$ was 12% and 11% of that in wild-type ES cells treated, respectively (Fig. 4, lanes 5 and 6). JNK activity in $mkk7^{-/-}$ ES cells treated with $CdCl_2$ and $HgCl_2$ was 44% and 22% of that in wild-type ES cells treated, respectively (Fig. 4, lanes 8 and 9). Determination of JNK activity based on [$\gamma - {}^{32}P$] incorporation into GST-c-Jun also showed the significant reduction of $CdCl_2$-induced JNK activation in both, $mkk4^{-/-}$ and $mkk7^{-/-}$ ES cells (Nakagawa et al., unpublished data).

4. Discussion

The present study showed that treatment with $CdCl_2$ or $HgCl_2$ induced the accumulation of phosphorylated form of JNK in a dose- and time-dependent manner in wild-type ES cells as has been observed in the various cell types (Matsuoka and Igisu, 2002). In both, $mkk4^{-/-}$ and $mkk7^{-/-}$ ES cells which lack an upstream JNK activator, $CdCl_2$- or $HgCl_2$-induced phosphorylation and activation of JNK were suppressed dramatically. However, in $mkk7^{-/-}$ ES cells treated with $CdCl_2$ and $HgCl_2$, JNK activation was not abolished (suppressed by 56% and 78%, respectively). On the other hand, significant phosphorylation of other members of MAPK, p38 and ERK, was retained in

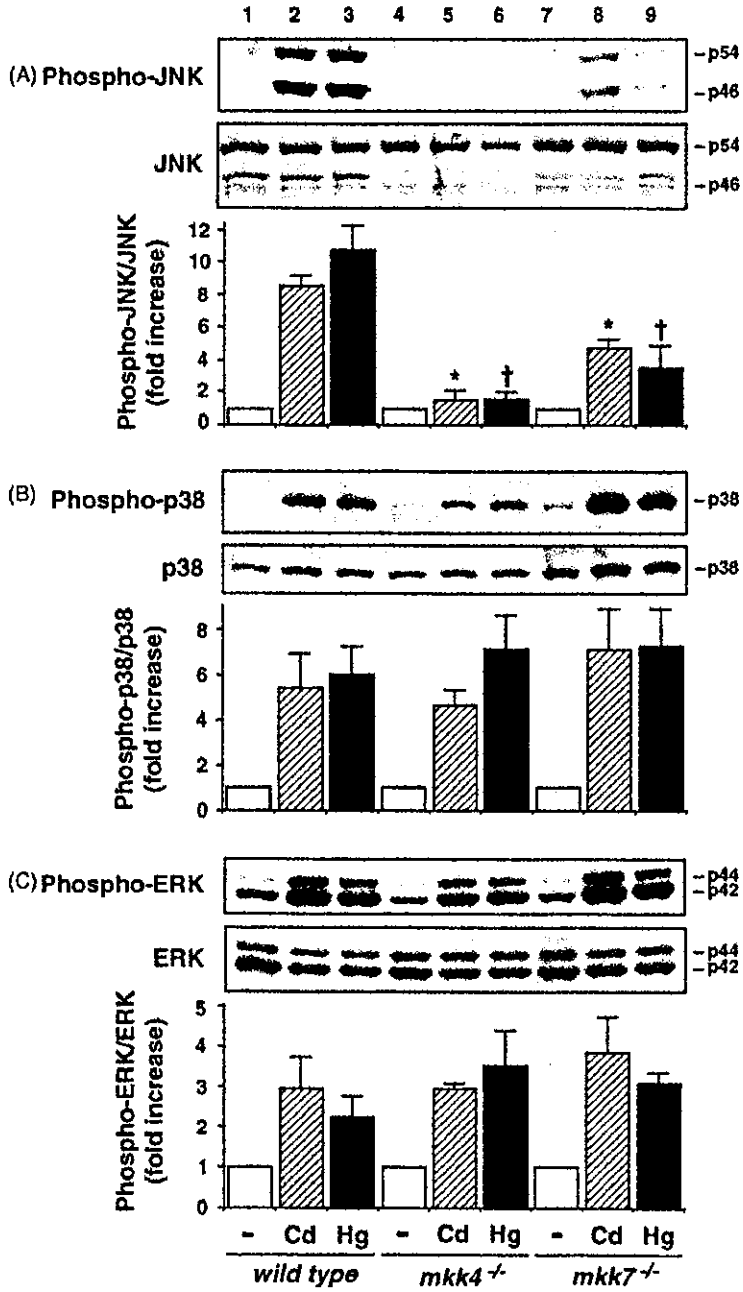

Fig. 3. Effects of $CdCl_2$ or $HgCl_2$ treatment on the levels of phosphorylated JNK (A), phosphorylated p38 (B), and phosphorylated ERK (C). Wild-type, *mkk4*$^{-/-}$ and *mkk7*$^{-/-}$ ES cells were incubated with serum-free medium (lanes 1, 4, and 7), 20 μM $CdCl_2$ (lanes 2, 5, and 8) or 20 μM $HgCl_2$ (lanes 3, 6, and 9) for 1 h, and cell lysates were subjected to immunoblotting using anti-phospho-JNK and anti-JNK antibodies (A), anti-phospho-p38 and anti-p38 antibodies (B), and anti-phospho-ERK and anti-ERK antibodies (C). Results shown are representative immunoblot and densitometric analysis of phosphorylated JNK, p38 and ERK. Each value was expressed as the ratio of phosphorylated MAPK level to the corresponding total MAPK level, and the value of control (without metal treatments) was set to one. Each column and bar represent the mean ± S.D. of three independent experiments. $^{*}P < 0.01$ compared to wild-type ES cells treated with $CdCl_2$, $^{\dagger}P < 0.01$ compared to wild-type ES cells treated with $HgCl_2$.

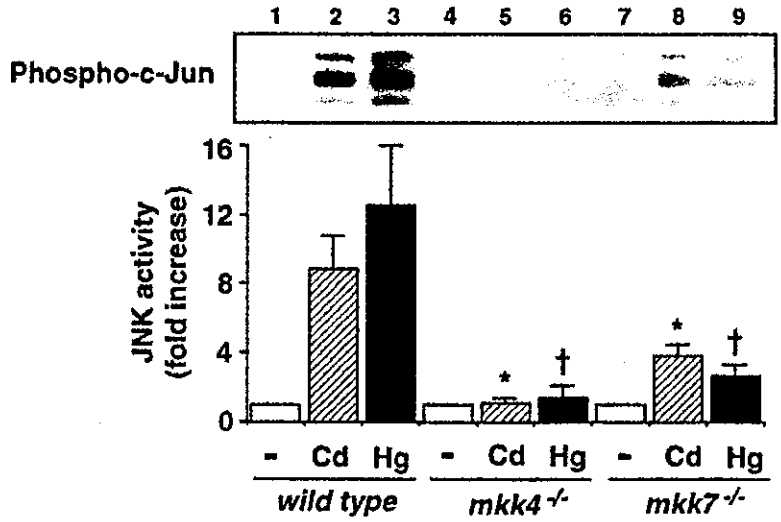

Fig. 4. Effects of $CdCl_2$ or $HgCl_2$ treatment on the activity of JNK in wild-type, *mkk4*$^{-/-}$ and *mkk7*$^{-/-}$ ES cells. Wild-type, *mkk4*$^{-/-}$ and *mkk7*$^{-/-}$ ES cells were incubated with serum-free medium (lanes 1, 4, and 7), 20 μM $CdCl_2$ (lanes 2, 5, and 8) or 20 μM $HgCl_2$ (lanes 3, 6, and 9) for 1 h, and cell lysates were used for in vitro kinase reaction with GST-c-Jun (1–89) as substrate. Phosphorylation of GST-c-Jun was analyzed with immunoblotting using anti-phospho-c-Jun antibody. Results shown are representative immunoblot and densitometric analysis of phosphorylated c-Jun. Each value was expressed as the fold increase with respect to the corresponding control (without metal treatments). Each column and bar represent the mean ± S.D. of four independent experiments. $^{*}P < 0.01$ compared to wild-type ES cells treated with $CdCl_2$. $^{\dagger}P < 0.01$ compared to wild-type ES cells treated with $HgCl_2$.

these mutated cell lines. These findings suggest that the full activation of JNK by toxic metal exposure requires both MKK4 and MKK7, and these upstream kinases might contribute differentially in JNK activation between ES cells exposed to $CdCl_2$ and $HgCl_2$. $CdCl_2$-induced JNK activation seems to depend on MKK4 more extensively than MKK7.

In contrast, previous studies using cells transfected with dominant-negative form of MKK4 or MKK7 showed that cadmium might activate JNK through MKK7, but not MKK4. Transfection with MKK4 mutant elevated $CdCl_2$ (80 μM, 3 h exposure) -induced JNK activation 1.9-fold in human non-small-cell lung carcinoma cells, while expression of MKK7 mutant reduced JNK activity by 35% (Chuang and Yang, 2001). However, expression of MKK7 mutant failed to suppress JNK activity in the same cells treated with a higher concentration of $CdCl_2$ (130 μM) (Chuang et al., 2000). In rat mesangial cells, $CdCl_2$ (10 μM, 8 h exposure) -induced JNK activation was suppressed by 53% when transfected with MKK7 mutant, but not changed by expression of MKK4 mutant (Ding and Templeton, 2000). On the other hand, it has been reported that treatment with $CdCl_2$ induced the phosphorylation of MKK4 in Rat-1 fibroblasts (Iordanov and Magun, 1999), and we also found the phosphorylation of MKK4 on Thr^{261} in wild-type ES cells following exposure to $CdCl_2$ or $HgCl_2$ (data not shown). Thus, MKK4 could be activated by upstream kinase (i.e., MAPK kinase kinase) in response to $CdCl_2$ or $HgCl_2$ exposure, and disruption of the *mkk4* gene abolished toxic metal-induced JNK activation almost completely in ES cells. While the precise functions of MKK4 and MKK7 in cells exposed to toxic metal are still not clear, these MAPK kinases might play a different role in JNK activation depending on the cell type and the experimental condition of exposure. With respect to mkk4$^{-/-}$ and *mkk7*$^{-/-}$ ES cells exposed to $CdCl_2$ or $HgCl_2$, the roles of splice variants and the effects of JNK (p46) expression remain to be examined.

In summary, as has been shown in various stress-induced JNK activation (Kishimoto et al., 2003; Wada et al., 2001), both MKK4 and MKK7 were required for the full activation of JNK in mouse ES cells exposed to $CdCl_2$ or $HgCl_2$. The *mkk4*$^{-/-}$ and *mkk7*$^{-/-}$ ES cells seem to be useful to analyze functions and signaling pathway of JNK activation induced by environmental stresses including toxic metals.

Acknowledgements

We thank Takeo Okuno for technical help. This work was supported in part by Grant-in-Aid for Scientific Research (KAKENHI: 14570313 and 14570315) from the Ministry of Education, Culture, Sports, Science and Technology (MEXT), Japan.

References

Chang, L., Karin, M., 2001. Mammalian MAP kinase signalling cascades. Nature 410, 37–40.

Chuang, S.-M., Yang, J.-L., 2001. Comparison of roles of three mitogen-activated protein kinases induced by chromium (VI) and cadmium in non-small-cell lung carcinoma cells. Mol. Cell. Biochem. 222, 85–95.

Chuang, S.-M., Wang, I.-C., Yang, J.-L., 2000. Roles of JNK, p38 and ERK mitogen-activated protein kinases in the growth inhibition and apoptosis induced by cadmium. Carcinogenesis 21, 1423–1432.

Cobb, M.H., Goldsmith, E.J., 1995. How MAP kinases are regulated. J. Biol. Chem. 270, 14843–14846.

Ding, W., Templeton, D.M., 2000. Stress-activated protein kinase-dependent induction of *c-fos* by Cd^{2+} is mediated by MKK7. Biochem. Biophys. Res. Commun. 273, 718–722.

Iordanov, M.S., Magun, B.E., 1999. Different mechanisms of c-Jun NH_2-terminal kinase-1 (JNK1) activation by ultraviolet-B radiation and by oxidative stressors. J. Biol. Chem. 274, 25801–25806.

Kishimoto, H., Nakagawa, K., Watanabe, T., Kitagawa, D., Momose, H., Seo, J., Nishitai, G., Shimizu, N., Ohata, S., Tanemura, S., Asaka, S., Goto, T., Fukushi, H., Yoshida, H., Suzuki, A., Sasaki, T., Wada, T., Penninger, J.M., Nishina, H., Katada, T., 2003. Different properties of SEK1 and MKK7 in dual phosphorylation of stress-induced activated protein kinase SAPK/JNK in embryonic stem cells. J. Biol. Chem. 278, 16595–16601.

Kyriakis, J.M., Avruch, J., 1996. Sounding the alarm: protein kinase cascades activated by stress and inflammation. J. Biol. Chem. 271, 24313–24316.

Lawler, S., Fleming, Y., Goedert, M., Cohen, P., 1998. Synergistic activation of SAPK1/JNK1 by two MAP kinase kinases in vitro. Curr. Biol. 8, 1387–1390.

Matsuoka, M., Igisu, H., 1998. Activation of c-Jun NH_2-terminal kinase (JNK/SAPK) in LLC-PK_1 cells by cadmium. Biochem. Biophys. Res. Commun. 251, 527–532.

Matsuoka, M., Igisu, H., 2002. Effects of heavy metals on mitogen-activated protein kinase pathways. Environ. Health Prev. Med. 6, 210–217.

Matsuoka, M., Wispriyono, B., Iryo, Y., Igisu, H., 2000. Mercury chloride activates c-Jun N-terminal kinase and induces *c-jun* expression in LLC-PK_1 cells. Toxicol. Sci. 53, 361–368.

Nishina, H., Fischer, K.D., Radvanyi, L., Shahinian, A., Hakem, R., Rubie, E.A., Bernstein, A., Mak, T.W., Woodgett, J.R., Penninger, J.M., 1997. Stress-signalling kinase Sek1 protects thymocytes from apoptosis mediated by CD95 and CD3. Nature 385, 350–353.

Robinson, M.J., Cobb, M.H., 1997. Mitogen-activated protein kinase pathways. Curr. Opin. Cell Biol. 9, 180–186.

Wada, T., Nakagawa, K., Watanabe, T., Nishitai, G., Seo, J., Kishimoto, H., Kitagawa, D., Sasaki, T., Penninger, J.M., Nishina, H., Katada, T., 2001. Impaired synergistic activation of stress-activated protein kinase SAPK/JNK in mouse embryonic stem cells lacking SEK1/MKK4: different contribution of SEK2/MKK7 isoforms to the synergistic activation. J. Biol. Chem. 276, 30892–30897.

Weston, C.R., Davis, R.J., 2002. The JNK signal transduction pathway. Curr. Opin. Genet. Dev. 12, 14–21.

Yu, Z., Matsuoka, M., Wispriyono, B., Iryo, Y., Igisu, H., 2000. Activation of mitogen-activated protein kinases by tributyltin in CCRF-CEM cells: role of intracellular Ca^{2+}. Toxicol. Appl. Pharmacol. 168, 200–207.

ELSEVIER

Mechanisms of Development 121 (2004) 647–658

www.elsevier.com/locate/modo

Research paper

A systematic genome-wide screen for mutations affecting organogenesis in Medaka, *Oryzias latipes*

Makoto Furutani-Seiki[a,*], Takao Sasado[a], Chikako Morinaga[a], Hiroshi Suwa[a], Katsutoshi Niwa[a], Hiroki Yoda[b], Tomonori Deguchi[b], Yukihiro Hirose[c], Akihito Yasuoka[d], Thorsten Henrich[a], Tomomi Watanabe[e], Norimasa Iwanami[f], Daiju Kitagawa[e], Kota Saito[e], Satoshi Asaka[e], Masakazu Osakada[g], Sanae Kunimatsu[f], Akihiro Momoi[b], Harun Elmasri[h], Christoph Winkler[h], Mirana Ramialison[a], Felix Loosli[i], Rebecca Quiring[i], Matthias Carl[i], Clemens Grabher[i], Sylke Winkler[i], Filippo Del Bene[i], Ai Shinomiya[j], Yasuko Kota[a], Toshiyuki Yamanaka[a], Yasuko Okamoto[a], Katsuhito Takahashi[g], Takeshi Todo[k], Keiko Abe[d], Yousuke Takahama[f], Minoru Tanaka[l], Hiroshi Mitani[m], Toshiaki Katada[e], Hiroshi Nishina[e], Noboru Nakajima[a], Joachim Wittbrodt[i], Hisato Kondoh[a,b,*]

[a]*Japan Science and Technology Corporation, Kondoh Differentiation Signaling Project, Kawaaracho 14, Yoshida, Sakyoku, Kyoto 606-8305, Japan*
[b]*Graduate School of Frontier Biosciences, Osaka University, Osaka 565-0871, Japan*
[c]*Graduate School of Biostudies, Kyoto University, Kyoto 606-8502, Japan*
[d]*Graduate School of Agricultural and Life Sciences, The University of Tokyo, Tokyo 113-0033, Japan*
[e]*Department of Physiological Chemistry, Graduate School of Pharmaceutical Sciences, The University of Tokyo, Tokyo 113-0033, Japan*
[f]*Division of Experimental Immunology, Institute for Genome Research, The University of Tokushima, Tokushima 770-8503, Japan*
[g]*Department of Molecular Medicine and Pathophysiology, Research Institute, Osaka Medical Center for Cancer and Cardiovascular Diseases, Osaka 537-8511, Japan*
[h]*Physiological Chemistry I, Biocenter, University of Wuerzburg, D-97074 Wuerzburg, Germany*
[i]*Developmental Biology Programme, EMBL Heidelberg, D-69117 Heidelberg, Germany*
[j]*Department of Environmental Science, Faculty of Science, Niigata University, Niigata 950-2181, Japan*
[k]*Radiation Biology Center, Kyoto University, Kyoto 606-8501, Japan*
[l]*Division of Biological Sciences, Graduate School of Sciences, Hokkaido University, Hokkaido 060-0808, Japan*
[m]*Department of Integrated Biosciences, Graduate School of Frontier Sciences, The University of Tokyo, Chiba 277-8562, Japan*

Received 1 February 2004; received in revised form 22 March 2004; accepted 21 April 2004

Abstract

A large-scale mutagenesis screen was performed in Medaka to identify genes acting in diverse developmental processes. Mutations were identified in homozygous F3 progeny derived from ENU-treated founder males. In addition to the morphological inspection of live embryos, other approaches were used to detect abnormalities in organogenesis and in specific cellular processes, including germ cell migration, nerve tract formation, sensory organ differentiation and DNA repair. Among 2031 embryonic lethal mutations identified, 312 causing defects in organogenesis were selected for further analyses. From these, 126 mutations were characterized genetically and assigned to 105 genes. The similarity of the development of Medaka and zebrafish facilitated the comparison of mutant phenotypes, which indicated that many mutations in Medaka cause unique phenotypes so far unrecorded in zebrafish. Even when mutations of the two fish species cause a similar phenotype such as *one-eyed-pinhead* or *parachute*, more genes were found in Medaka than in zebrafish that produced the same phenotype when mutated. These observations suggest that many Medaka mutants represent new genes and, therefore, are important complements to the collection of zebrafish mutants that have proven so valuable for exploring genomic function in development.

Keywords: Medaka; Mutants; Interspecies difference; ENU mutagenesis; Vertebrate organogenesis; Kyoto screen

* Corresponding authors. Tel.: +81-75-771-9362; fax: +81-75-771-8281.
E-mail addresses: furutaniseiki@dsp.jst.go.jp (M. Furutani-Seiki), j61056@hpc.cmc.osaka-u.ac.jp (H. Kondoh).

0925-4773/$ - see front matter © 2004 Published by Elsevier Ireland Ltd.
doi:10.1016/j.mod.2004.04.016

1. Introduction

Mutants serve as an important entry point to the understanding of gene function. In particular, systematic screening for mutations among a mutagenized population of model organisms has been a powerful approach to identifying genes and their functions involved in specific cellular processes. The assignment of individual genes responsible for mutations has been greatly facilitated by recent advances in genomic research (e.g. physical maps and whole-genome sequencing). This approach has been particularly useful in revealing the ontogenetic process, and was successfully applied to invertebrate animals and plants, such as *Drosophila melanogaster*, *Caenorhabditis elegans*, and *Arabidopsis thaliana* (Nüsslein-Volhard and Wieschaus, 1980; Brenner, 1974; Mayer, 1991).

Among vertebrates, small fish are suitable for mutational investigations, for their ease of rearing in a relatively compact space, reasonably short generation time and, in particular, the translucent embryos they produce. In many species, embryos develop outside the mothers' body rendering them easy to inspect visually and to manipulate their tissues and cells (refer to Kimmel, 1989). One such fish is the zebrafish, *Danio rerio*; the accomplishment of large-scale mutagenesis screens (Haffter et al., 1996; Driever et al., 1996) and use of mutants to study developmental processes carried out in the past two decades have established the zebrafish as the premier vertebrate for unbiased analyses of genomic functions in development.

However, the use of a single species for mutagenesis screening will not be sufficient to uncover all gene functions, partly because of functional overlap among related genes, which is a common feature of vertebrates. This problem may be alleviated by the use of a second fish species where usage of genes may vary subtly from zebrafish. We therefore adopted Medaka as another fish species for large-scale identification and recovery of mutations. Medaka, *Oryzias latipes*, has been used as an experimental model animal since the 1920s (Aida, 1921). Sex chromosome-dependent sex determination (Aida, 1921), demonstration of hormone-induced sex reversal (Yamamoto, 1965) and identification of the sex determining gene DMY (Matsuda et al., 2002; Nanda et al., 2002) made this fish species a good model to study the mechanisms of sexual differentiation. Genetic tools have been generated including established inbred strains (Hyodo-Taguchi et al., 1983), a fine-scale genetic map derived from polymorphic markers (Naruse et al., 2000) and quantitative trait loci (Ishikawa, 2000). Medaka has a small genome size (one-half of that of zebrafish and only twice that of Fugu) and is phylogenically distant from zebrafish, diverging about 110 million years ago (Wittbrodt et al., 2002), making it useful for comparisons of conserved and divergent gene functions in teleost evolution (Ohno, 1970; Amores et al., 1998).

Small-scale pilot screens for mutations affecting the development of the eyes and nervous system (Loosli, et al., 2000; Ishikawa, 2000) suggested a significantly different spectrum of mutant phenotypes from those described for zebrafish and provided encouragement for expanded mutagenesis screening using Medaka.

In this overview paper, we summarize the results of a large-scale systematic screen for mutations in Medaka. The major focus of this mutant screen was on embryonic pattern formation and organogenesis. In addition to morphological criteria, a variety of labeling techniques were used to detect abnormalities in specific cellular features or cell behaviors. The Kyoto collection of Medaka mutants will complement and extend analyses on zebrafish and mouse mutants (Hrabe de Angelis et al., 2000; Nolan et al., 2000) and expand our understanding of general mechanisms underlying organogenesis.

2. Results

2.1. Overall design of mutagenesis screen

We carried out a large-scale mutagenesis screen to detect mutations that produce defects ranging from early body patterning to cellular differentiation and organ formation. In addition to morphological criteria, various screening procedures were used to detect more subtle abnormalities in specific structures or functional processes. Germ line cells, thymocytes, optic, cranial and lateral line nerves, and optic tectal projections of retinal ganglion cell (RGC) axons were visualized by in situ hybridization, immunostaining or fluorescent dye injection in fixed embryos. In addition, the potential for DNA repair and bilirubin and lipid metabolism associated with liver function were examined.

An essential step in a large-scale mutagenesis screen is to start with a wild-type strain suitable for identifying zygotic, recessive mutations. After brother–sister mating from the Cab strain (Wittbrodt et al., 2002) for more than nine generations, a substrain (Kyoto-Cab strain) was selected for high fecundity and a low background of abnormal embryonic development. A three-generation in-crossing scheme was used to generate F3 embryos homozygous for mutations induced in founder males (Fig. 1).

To introduce mutations into the germ line, male founder adult fish were treated with ENU (*N*-ethyl-*N*-nitrosourea) (Shima and Shimada, 1988), which has been used for mutagenesis in zebrafish (Mullins et al., 1994; Solnica-Krezel et al., 1994) and mice (Russell and Montgomery, 1982). ENU is known to introduce point mutations very efficiently and relatively randomly in spermatogonia (Russell and Montgomery, 1982). Crossing ENU-treated founder males with albino mutant females (specific locus test) indicated the efficiency of mutagenesis ranged from 1/196 to 1/726 under the conditions employed (refer to Section 4).

We raised ca. 1300 F2 families, and used 1137 F2 families to produce the potentially homozygous F3 embryos

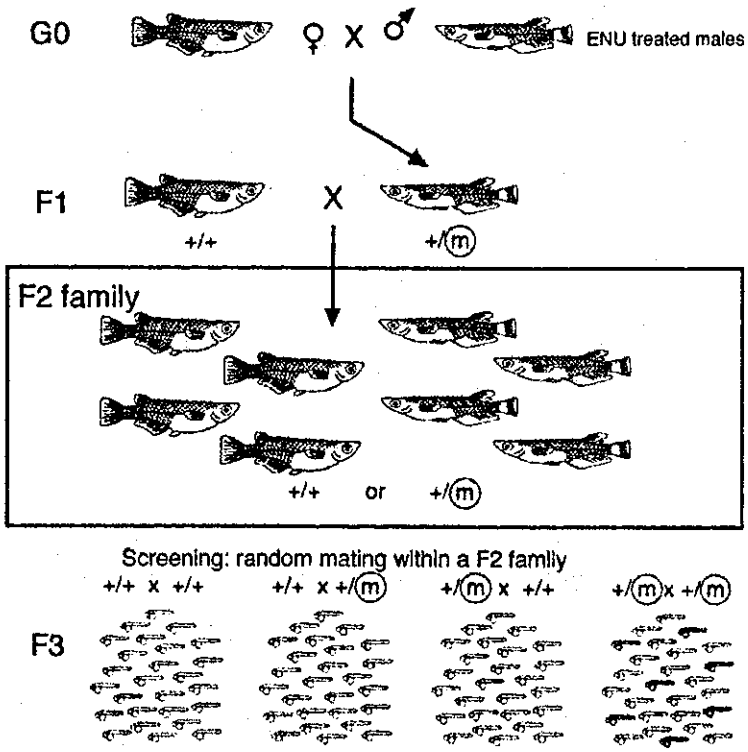

Fig. 1. A scheme of breeding of mutagenized fish population to identify recessive mutations (Adopted from Haffter et al., 1996, with modification). Males 4 weeks after treatment with ENU were mated with wild-type females to produce F1 progeny, which are heterozygous carriers of mutations derived from the mutagenized paternal genome. Many pairs of F1 fish were mated to generate F2 families, each consisting of about 60 fish derived from a single pair. A mutation designated as m harbored in an F1 parent is transmitted to one-half of the F2 families. Random brother–sister mating within an F2 family is expected to produce homozygotes of the mutation at a frequency of 1/4, assuming that the Mendelian ratio applies: When both F2 parents are heterozygous for mutation m, one-fourth of their F3 progeny will be homozygous for m and exhibit the mutant phenotype (shown on the right side).

bearing mutations. Of the more than 6700 F2 pairs mated, 6088 intercross pairs successfully produced progeny, and 24,887 clutches (a set of eggs produced per mating) were used for mutant screening. Nearly 260,000 F3 embryos were inspected during the screen. In total, 1588 mutagenized haploid genomes were screened for recessive mutations.

2.2. Detection of mutant phenotypes

Screening for morphological abnormalities in live embryos was performed at three stages of development, namely st. 19–21 (27–34 hpf, hours post-fertilization), st. 25–27 (50–58 hpf) and st. 32–35 (4 dpf, days post-fertilization) (Fig. 2). The earliest stage was chosen for identifying defects in early embryonic patterning, including gastrulation, dorso-ventral polarity, body axis formation, and early tissue degeneration. Screening at the second time point focused on the rudiments of organs, such as the eye vesicles, brain, heart primordium, otic vesicles, somites and notochord. At the third time point, abnormalities in organ morphogenesis were detected by screening the olfactory bulbs, brain ventricles, otic vesicles, liver, heart, vasculature, and pectoral fin buds. Special attention was paid to morphological abnormalities accompanied by cell degeneration, since specific patterning defects can produce localized cell degeneration at later stages (Furutani-Seiki et al., 1996).

While zebrafish lay about 100 eggs once in 1–2 weeks, Medaka spawns 10–40 eggs daily. We thus collected embryos from each pair for five consecutive days per week over two-week period, and used these different clutches of embryos in multiple assays. This feature of the Medaka system enabled simultaneous inspection of different clutches of embryos from the same parental pair at staggered developmental stages. Simultaneous observation of embryos at different ages but derived from the same parents also provided confirmation that abnormalities were genetic rather than the result of compromised egg quality.

Phenotypes affecting specific cell types were assessed by labeling of whole-mount specimens of fixed embryos using tissue-specific riboprobes (Fig. 3). In situ hybridization with a vasa probe allowed the visualization of primordial germ cells (Fig. 3A,A′) and differentiated germ cells (Fig. 3B,B″) at st. 26 (59 hpf) and 15 dpf, respectively (Shinomiya et al.,

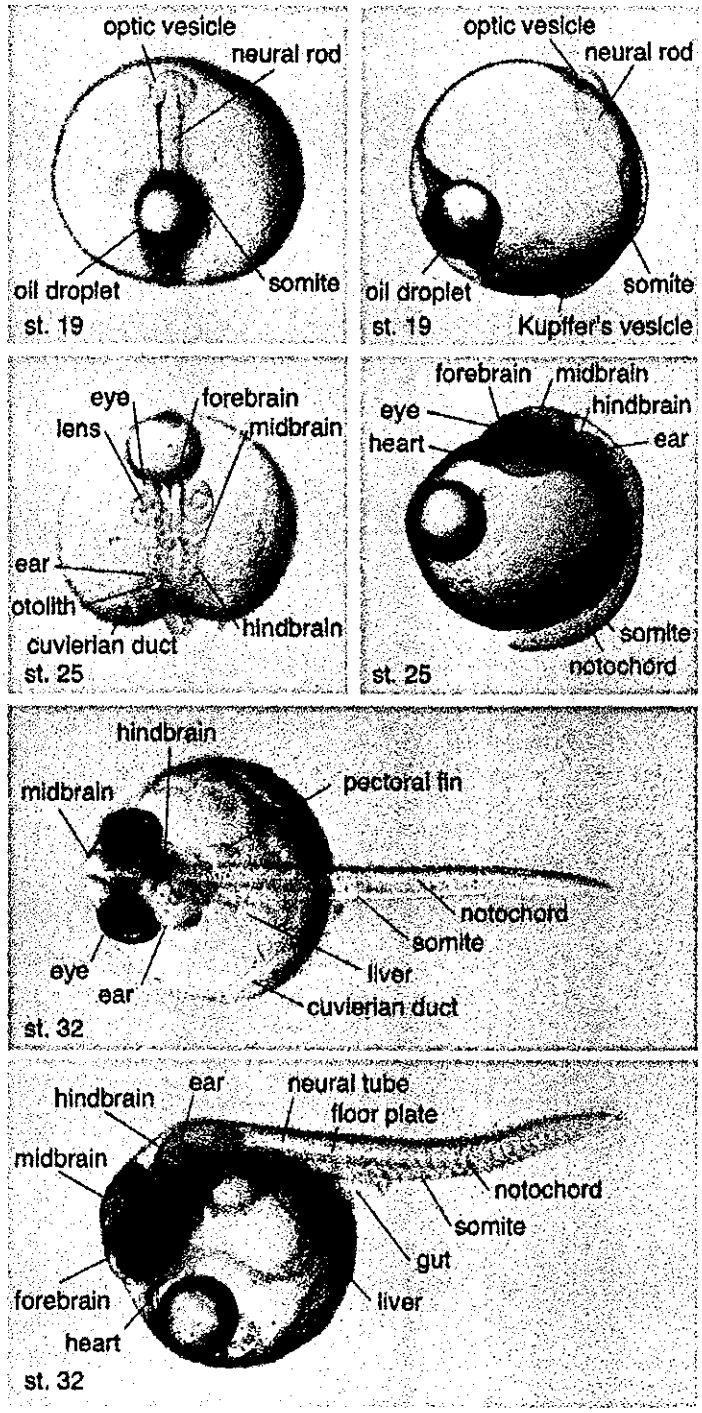

Fig. 2. Images of live Medaka embryos at three developmental stages when mutants were screened by morphological criteria. Visible structures in live embryos are marked.

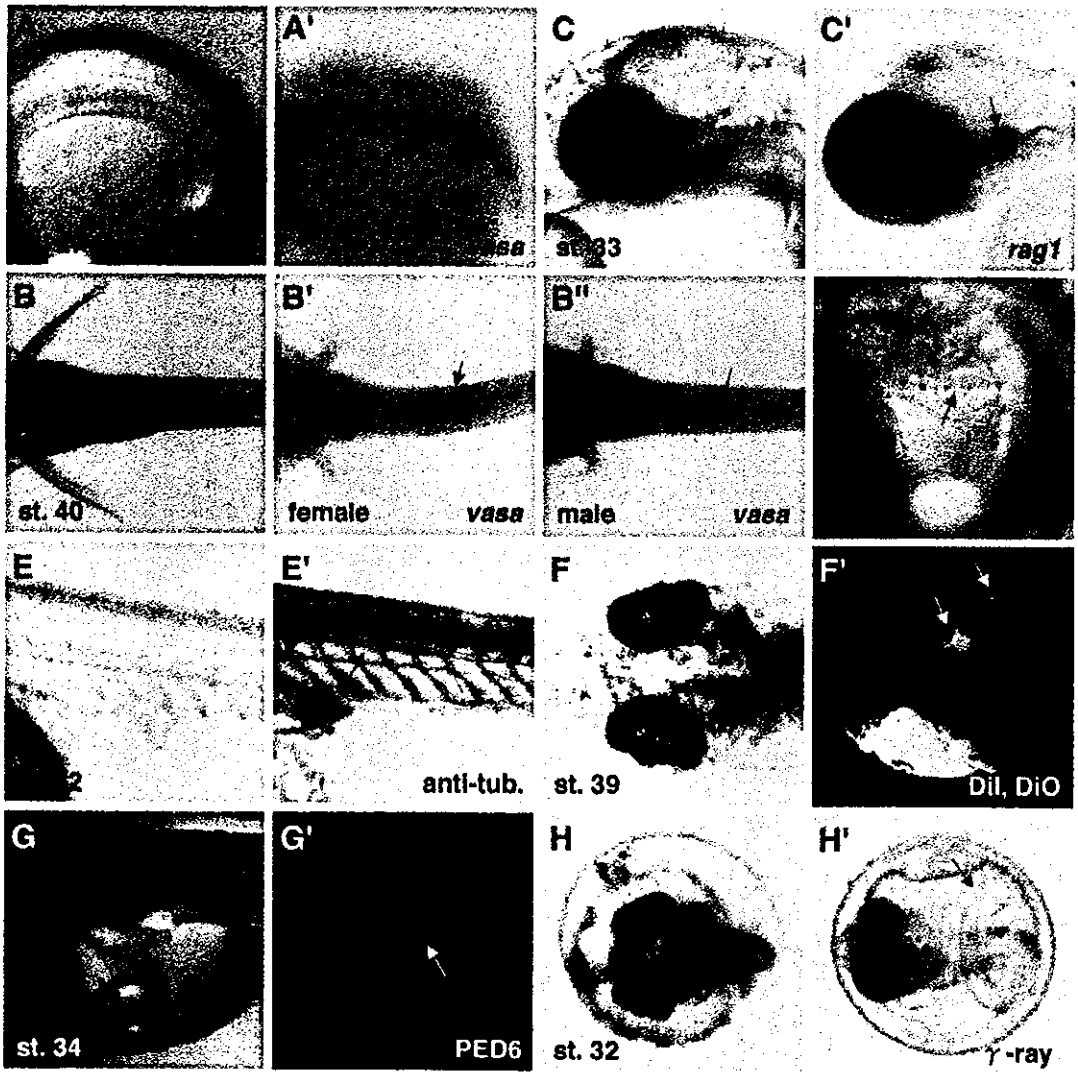

Fig. 3. Various assays employed in screening of Medaka mutants. (A, A′) St. 27 embryos, (A) live and (A′) *vasa* in situ hybridization detecting PGCs (arrow) colonizing in the gonad area of the trunk. (B. B′, B″) Early larva at st. 40, (B) live and (B′, B″) *vasa* in situ hybridization of st. 40 larvae, showing gonads containing abundant *vasa*-positive germ cells (arrow). A female larva (B′) usually has a larger right gonad than a male (B″). (C, C′) Anterior part of st. 33 embryos, (C) live and (C′) *rag1* in situ hybridization showing the location of thymus (arrow). (D) St. 34 live embryo, metabolism of hemoglobin to bilirubin was monitored by the color of bile in the gall bladder (arrow). (E, E′) Posterior part of st. 32 embryos, (E) live embryo and (E′) posterior lateral line nerves (arrow) visualized by immunostaining of acetylated tubulin and HNK-1 epitope. (F, F′) St. 39 larvae that have just hatched, (F) a live larva, (F′) labeling RGC axons projecting to foci of the contralateral tectum (arrows) by injecting lipophilic fluorescent dyes, DiI and DiO in the retina at fixed retinal positions. (G, G′) A live embryo at st. 34 loaded with PED6 and showing accumulation of its fluorescent metabolites in the gall bladder, under bright field illumination (G) and in fluorescent image (arrow) (G′). (H, H′) Effect of γ-ray irradiation on embryogenesis. (H) A wild-type embryo with a chorion at st. 32 recovered from irradiation with a semi-lethal dose of γ-ray at st.24. (H′) A homozygous γ-ray-sensitive mutant (*ric1*) showing a curled tail (arrow), characteristic indication of γ-ray sensitivity. (A, A′) semi-lateral view; (B-B″) ventral view; (C, C′, D, E, E′, G, G′) lateral view; (F, F′, H, H′) dorsal view.

2000). The *rag1* probe was used to detect thymocytes in st. 32 embryos (Fig. 3C,C′). Immunostaining using a mixture of anti-acetylated tubulin and HNK1 antibodies was performed to detect axons forming cranial and lateral line nerves at st. 32 (Fig. 3E,E′). The topographic projection of axons from RGCs to the optic tectum was visualized by injecting DiI and DiO at the ventrotemporal and dorsonasal positions, respectively, of retinas, as previously described in a screen for zebrafish retinotectal mutants (Fig. 3F,F′) (Baier et al., 1996).

Liver-associated physiological activity involving bile and lipid metabolism was scored by bile color (Fig. 3D) and the accumulation of a fluorescent metabolite of PED6, a phospholipase A_2 substrate (Farber et al., 2001), in the gall

Table 1
Numerical record of mutations identified in the Kyoto Medaka screen

Mutants	Number	Percentage
Total lethal mutations identified[a]	2031	100
F3 progeny raised	372	18
Newly discovered mutations in the F3 progeny	21	1.0
Mutations confirmed and recovered	312	15
Mutations not confirmed in the F3 progeny	39	1.9
Mutations lost during rearing F3 progeny	45	2.2
Mutations already assigned to genes	126	6.2
Mutations in the process of gene assignment	186	9.1

[a] Confirmed by repeated occurrences of the same phenotype in different clutches from the same parental pair.

bladder in living embryos (Fig. 3G,G′). DNA repair activity during embryogenesis was tested by examining recovery after exposure of developing embryos to a sublethal dose of γ-ray radiation (Fig. 3H,H′).

Together, using all of the screening methods, a total of 2031 embryonic lethal mutations were identified (Table 1). As Medaka embryos hatch at 9 dpf at 28 °C, mutant embryos that failed to hatch by this time were defined as carrying embryonic lethal mutations. Among these mutations, we selected 372 for further analyses on the basis of their specific phenotypes. F2 parents carrying the mutations of interest were outcrossed to wild-type fish and the F3 progeny raised and used for reidentification and recovery of mutations. The remaining mutations caused (1) non-specific general abnormalities, such as overall degeneration, retardation and edema as reported previously in zebrafish (Mullins et al., 1994; Solnica-Krezel et al., 1994) or (2) more specific phenotypes that were also accompanied by generalized retardation or degeneration. From the F3 generation, a total of 312 mutations were recovered and subjected to more detailed characterization.

2.3. Mutant classification and complementation analysis

Mutations recovered from the F3 generation were grouped into several classes according to the phenotype of homozygous mutants (Table 2). Within a class, heterozygous carriers of independently isolated mutations were intercrossed to test for genetic complementation. Complementation testing was completed for 126 mutations, and indicated that these mutations define 105 distinct genetic loci.

Table 2
Summary of identified gene according to the affected tissues

Tissues affected by the mutations	Genomes screened	Genes (mutations)
Forebrain	1588	25 (33)
Primordial germ cells	450	10 (12)
Gonad	428	13 (16)
Lateral line	432	4 (4)
Liver	162	19 (22)
Thymus	502	13 (15)
Eye	529	22 (25)
Retino-tectal pathfinding	184	5 (7)
Somite	1588	9 (12)
γ-Ray sensitivity	780	3 (3)

2.4. Mutant phenotypes

2.4.1. Forebrain mutants

Formation of the forebrain was affected in 33 mutants of 25 genes (Kitagawa et al., 2004). The mutations were grouped into two major phenotypic classes: Group 1 included mutations in 11 genes that resulted in a reduced telencephalon and Group 2 mutations in 14 genes produced abnormal morphology of the telencephalon without significantly affecting its size. In zebrafish, the development of the telencephalon is affected in *knollnase* (*kas*), *masterblind* (*mbl*) and *silberblick* (*slb*) embryos (Heisenberg et al., 1996), and mutants associated with midline defects resulting in cyclopia or a curly tail down phenotype (Brand et al., 1996). Mutations in Medaka affecting forebrain formation appear distinct from those in zebrafish as judged by their morphology (Fig. 4), although a careful comparison of Medaka and zebrafish mutant phenotypes using specific markers is necessary to confirm this observation. As noted above, tissue degeneration

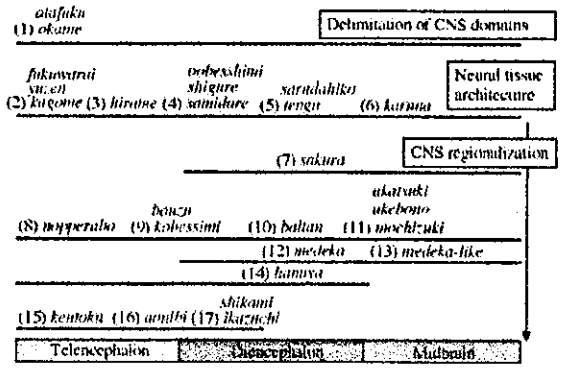

Fig. 4. Schematic presentation of Medaka mutations affecting anterior CNS and possible correspondence with the phenotypes of zebrafish mutants. Medaka mutants are roughly classified into 17 groups according to their phenotype, and the regions of CNS affected by the group of mutations are indicated by horizontal lines. Possible defect at cellular and tissue levels featuring the phenotype is indicated in the square. Medaka mutants displaying phenotypes resembling those of zebrafish mutations are indicated in red. Group 4 mutants of three genes exhibit a phenotype similar to that of the *parachute* zebrafish mutant. Group 8 mutants of one gene show the phenotypes analogous to those of *masterblind* and *headless* mutants. Group 11 mutants of three genes display the phenotype resembling to those of *one-eyed-pinhead* zebrafish mutants. Remaining mutations, possibly representing unique phenotypes of Medaka mutations, are indicated in blue. The correspondence to zebrafish mutant phenotype is only authors' interpretation, and does not imply a genetic correspondence. This scheme is drawn merely to provide the readers with an overview of mutant phenotypes, and the details are not necessarily precise.